

Mechanism of CO₂ Hydrogenation on Pd/Al₂O₃ Catalysts: Kinetics and Transient DRIFTS-MS Studies

Xiang Wang,[†] Hui Shi,[†] Ja Hun Kwak,^{†,‡} and János Szanyi*,[†]

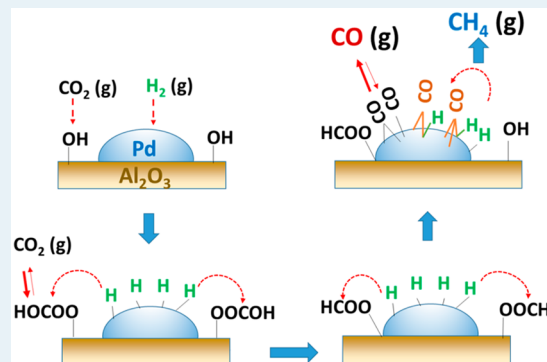
[†]Institute for Integrated Catalysis, Pacific Northwest National Laboratory, Richland, Washington 99352, United States

[‡]Department of Chemical Engineering, School of Energy and Chemical Engineering, UNIST, Ulsan 689-798, Korea

Supporting Information

ABSTRACT: The hydrogenation of CO₂ was investigated over a wide range of reaction conditions, using two Pd/γ-Al₂O₃ catalysts with different Pd loadings (5% and 0.5%) and dispersions (~11% and ~100%, respectively). Turnover rates for CO and CH₄ formation were both higher over 5% Pd/Al₂O₃ with a larger average Pd particle size than those over 0.5% Pd/Al₂O₃ with a smaller average particle size. The selectivity to methane (22–40%) on 5% Pd/Al₂O₃ was higher by a factor of 2–3 than that on 0.5% Pd/Al₂O₃. The drastically different rate expressions and apparent energies of activation for CO and CH₄ formation led us to conclude that reverse water gas shift and CO₂ methanation do not share the same rate-limiting step on Pd and that the two pathways are probably catalyzed at different surface sites. Measured reaction orders in CO₂ and H₂ pressures were similar over the two catalysts, suggesting that the reaction mechanism for each pathway does not change with particle size. In accordance, the DRIFTS results reveal that the prevalent surface species and their evolution patterns are comparable on the two catalysts during transient and steady-state experiments, switching feed gases among CO₂, H₂, and CO₂ + H₂. The DRIFTS and MS results also demonstrate that no direct dissociation of CO₂ takes place over the two catalysts and that CO₂ has to first react with surface hydroxyls on the oxide support. The thus-formed bicarbonates react with dissociatively adsorbed hydrogen on Pd particles to produce adsorbed formate species (bifunctional catalyst: CO₂ activation on the oxide support and H₂ dissociation on the metal particles). Formates near the Pd particles (most likely at the metal/oxide interface) can react rapidly with adsorbed H to produce CO, which then adsorbs on the metallic Pd particles. Two types of Pd sites are identified: one has a weak interaction with CO, which easily desorbs into gas phase at reaction temperatures, whereas the other interacts more strongly with CO, which is mainly in multibound forms and remains stable in He flow at high temperatures, but is reactive toward adsorbed H atoms on Pd leading eventually to CH₄ formation. 5% Pd/Al₂O₃ contains a larger fraction of terrace sites favorable for forming these more multibound and stable CO species than 0.5% Pd/Al₂O₃. Consequently, we propose that the difference in the formation rate and selectivity to CH₄ on different Pd particle sizes stems from the different concentrations of the reactive intermediate for the methanation pathway on the Pd surface.

KEYWORDS: CO₂ reduction, Pd/Al₂O₃, particle size, reaction mechanism, CO/CH₄ selectivity



1. INTRODUCTION

The utilization of CO₂, an increasingly attractive C1 building block, not only contributes to alleviating global climate changes induced by the increasing CO₂ emissions but also opens up new sustainable routes for synthesizing useful feedstock chemicals and fuels.¹ Catalytic hydrogenation is among the most important conversion pathways for CO₂, leading to a wide span of products (CO, CH₄, CH₃OH, HCOOH, and C₂+, depending on the reaction conditions and catalysts used.¹ At atmospheric pressure, CO₂ hydrogenation leads to CO (reverse water gas shift) and CH₄ (CO₂ methanation) as the only two C-containing products over most metal catalysts.

Over the past decades, considerable efforts, from both experiment and theory, have been devoted to understanding the site requirements and elementary steps of CO₂ hydrogenation over oxide-supported metal catalysts. However,

detailed reaction mechanisms and key intermediates of these processes are still under debate.^{2–8} A number of mechanisms have been proposed for CO₂ reduction to methane (methanation or the Sabatier reaction). They mainly fall into two categories: (1) dissociation of CO₂ to CO, followed by CO methanation,^{3,9–13} and (2) direct hydrogenation of CO₂ to methane without CO as an intermediate.^{14,15} However, the mechanism may vary depending on the pressures of both H₂ and CO₂, as well as the nature of the catalysts.¹

Regardless of the precise mechanism, the reaction requires the activation of both CO₂ and H₂. Park et al. found that on MgO-supported Pd catalysts, MgO initiates the reaction by

Received: July 13, 2015

Revised: August 20, 2015

Published: September 17, 2015

binding CO_2 , whereas the Pd particles dissociate H_2 and supply H atoms, actions essential for the further hydrogenation of carbonates to methane.^{3,4} Roger et al. found that on the ceria-zirconia catalysts, H_2 is dissociated on Ni sites while CO_2 is activated on the ceria-zirconia support to form carbonates which are hydrogenated into formates and further into methoxy species.¹⁶ Our recent work on alumina-supported Pd and Ru catalysts indicated that the Al_2O_3 support is responsible for the activation of CO_2 and the metal for the dissociation of H_2 .^{17,18} Furthermore, it was shown that large metallic Pd and Ru particles favor the formation of CH_4 , while smaller particles tend to produce more CO. The underlying principles governing these changes in product selectivity with metal particle size, however, were not understood. The present contribution mainly focuses on the mechanism of CO_2 hydrogenation over two Pd/ Al_2O_3 catalysts containing predominantly small and large Pd particles, as only a few scattered reports can be found on Pd-catalyzed CO_2 hydrogenation. We first present detailed kinetics obtained over a wide range of H_2 and CO_2 partial pressures. In situ diffuse reflectance infrared Fourier Transform (DRIFT) spectroscopy combined with mass spectrometric (MS) gas analysis was applied to shed light on the nature and role of surface intermediates during the catalytic reaction on different surface structures.

2. EXPERIMENTAL SECTION

Both 0.5 and 5 wt % Pd/ Al_2O_3 catalysts were prepared on a commercial γ - Al_2O_3 powder (Sasol, Puralox SBA-200, BET surface area = 200 m^2/g) by the incipient wetness method using $\text{Pd}(\text{NH}_3)_4(\text{NO}_3)_2$ as the precursor.¹⁷ After impregnation, the catalysts were dried at 373 K. The catalysts were activated prior to catalytic measurements by calcination at 773 K for 2 h under 6.7% O_2/He (flow rate = 60 mL/min) and followed by reduction at 773 K for 30 min under 2% H_2/Ar (flow rate = 60 mL/min).

The number of exposed Pd surface atoms was determined from the volumetric uptake of CO at 313 K, using a Micromeritics AutoChem 2920 Chemisorption Analyzer apparatus. The catalysts were pretreated under identical conditions to that applied prior to the catalytic tests. The number of accessible Pd sites was estimated using a Pd:CO = 1:1 stoichiometry ratio.

The catalytic reactions were carried out in a quartz, packed-bed tubular reactor (1/4 in. o.d. and 5/32 in. i.d.) with plug flow hydrodynamics. The catalysts were pressed, crushed, and sieved to 180–450 μm ; typically, 40 mg of catalyst was diluted by SiC to ensure better heat transfer and sufficient bed lengths which minimize channeling effects. Kinetics measurements were conducted in the temperature range of 513–593 K, at a total pressure of 101 kPa and a gas hourly space velocity (GHSV) of 45 000 $\text{cm}^3 \text{g}^{-1} \text{h}^{-1}$. The gas mixture fed into the reactor contained 10%–70% CO_2 and 70%–10% H_2 in He balance, at a total flow rate of 30 mL/min. All gases are of ultrahigh purity and further purified by additional oxygen and moisture traps (Supelpure-O Oxygen/Moisture Trap, Sigma-Aldrich). The conversion was kept at <5%. No activities were detected on bare supports or in an empty reactor. The absences of heat and diffusional limitations were confirmed by the method suggested by Koros and Nowak.¹⁹ Thermodynamic calculations also showed that both reaction pathways of CO_2 that form CO and CH_4 are remote from equilibrium under these conditions. The concentrations of reactants and products were measured with an Agilent HP 7820 gas chromatograph

equipped with a capillary column (Supelco, Carboxen 1010 PLOT, 30 m × 0.53 mm i.d.) and a thermal conductivity detector.

In situ IR spectra were collected on a Mattson Research Series 1000 FT-IR instrument equipped with a DRIFT accessory and a cell (Harrick). Each spectrum was recorded at 4 cm^{-1} resolution and was the average of 64 scans. The Pd/ Al_2O_3 sample was placed into the sample holder cup of the high temperature cell without packing or dilution. Then a background IR spectrum was taken at reaction temperature (513 K). Different mixtures of gases could be introduced into the cell, and the flow rates were controlled by electronic mass flow controllers (Brooks). For the transient experiments, pure He or the different mixtures at a total flow rate of 20 mL/min (2% CO_2 diluted in He, 8% H_2 diluted in He, 5% CO diluted in He and 2% CO_2 + 8% H_2 diluted in He, GHSV of 18 000 $\text{cm}^3 \text{g}^{-1} \text{h}^{-1}$) were switched and introduced to the cell. DRIFT spectra were recorded every ~90 s. The gases at the outlet of the cell were analyzed by a mass spectrometer by following the evolution of the m/z = 44 (CO_2), 2 (H_2), 15 (CH_4), 18 (H_2O), 28 (CO) with the response time of the mass spectrometer following a change in gas concentration being less than 1 s.

3. RESULTS

3.1. Reaction Kinetics. Pd dispersions estimated from CO chemisorption were ~100% and ~11% for the 0.5 and 5 wt % Pd/ Al_2O_3 catalysts, respectively, consistent with previous TEM characterization.¹⁷ Figure 1 shows the turnover frequencies

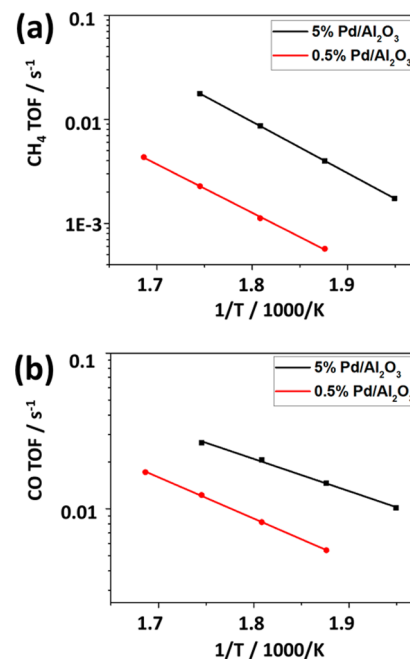


Figure 1. Turnover frequencies (TOFs) of (a) CH_4 and (b) CO formation as a function of reciprocal temperature at 513–593 K on 5% and 0.5% Pd/ Al_2O_3 in a flow containing 40% H_2 and 10% CO_2 in He balance (101 kPa total) at a total flow rate of 30 mL/min.

(TOFs) for CH_4 and CO formation (i.e., the rates of CH_4 and CO formation per surface Pd atom), plotted against reciprocal temperature (513–593 K), to obtain apparent activation energies at a molar ratio of $\text{H}_2/\text{CO}_2 = 4$ (the stoichiometric H_2/CO_2 ratio for CO_2 methanation). For the formation of both products, large Pd particles were catalytically more active than

small ones under these conditions. For example, at 553 K, the TOFs for CO formation were 8.2×10^{-3} and $2.1 \times 10^{-2} \text{ s}^{-1}$, while those for CH₄ formation were 1.1×10^{-3} and $8.6 \times 10^{-3} \text{ s}^{-1}$, on 0.5% and 5% Pd/Al₂O₃ catalysts, respectively. The selectivity to methane was 22–40% on 5% Pd/Al₂O₃, which was higher by a factor of 2–3 than that on 0.5% Pd/Al₂O₃ over the studied range of reaction temperature. The measured energy of activation was significantly lower for CO formation (40 and 45 kJ/mol on 5% and 0.5% Pd/Al₂O₃, respectively) than that for CH₄ formation (94 and 80 kJ/mol on 5% and 0.5% Pd/Al₂O₃, respectively).

The apparent activation energies were also determined for a wide range of partial pressures of H₂ and CO₂ (Figure 2). For

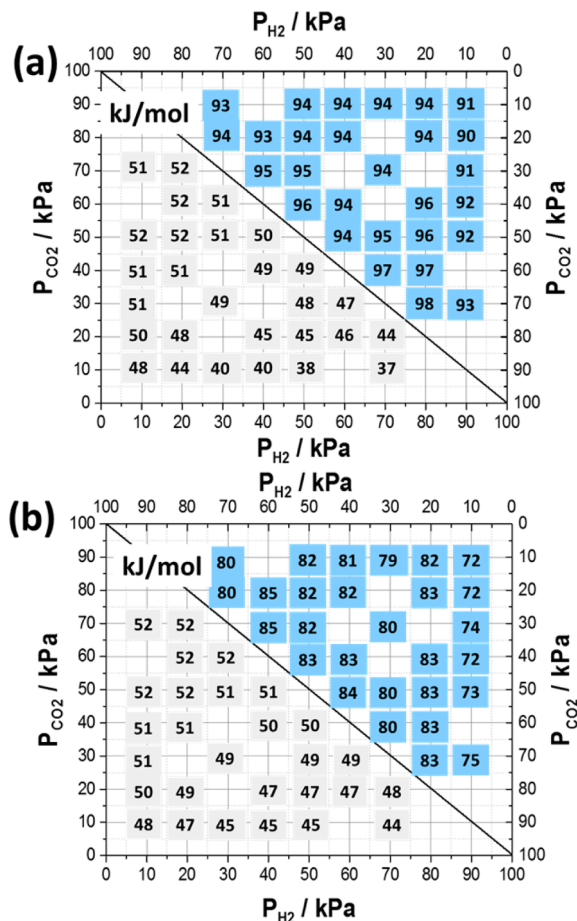


Figure 2. Apparent activation energies for CO formation (gray in lower left) and CH₄ formation (blue in upper right) in CO₂ hydrogenation over (a) 5% Pd/Al₂O₃ and (b) 0.5% Pd/Al₂O₃ under different partial pressures of H₂ and CO₂.

5% Pd/Al₂O₃, the apparent activation energy for CO formation decreased with increasing H₂ pressure (at a fixed CO₂ pressure) and decreasing CO₂ pressure (at a fixed H₂ pressure), varying from 52 to 37 kJ/mol. The apparent activation energy for CH₄ formation spanned a relatively narrow range from 90 to 98 kJ/mol (Figure 2a). In contrast, apparent activation energies for CO and CH₄ formation on 0.5% Pd/Al₂O₃ were much less sensitive to variations in both H₂ and CO₂ pressures. In addition, the measured activation energy for CH₄ formation over 0.5% Pd/Al₂O₃ (72–85 kJ/mol) was lower than that on 5% Pd/Al₂O₃, whereas the activation energy for CO (44–52 kJ/mol) was similar to that on 5% Pd/Al₂O₃.

Table 1 compiles the apparent reaction orders for CO formation in CO₂ and H₂ pressures on 5% and 0.5% Pd/Al₂O₃. At lower reaction temperatures, the reaction orders in CO₂ pressure remained almost unchanged (~0.46 on both catalysts) at any given H₂ pressure; this also held true for the reaction orders in H₂ (~0.22 on both catalysts) at any given CO₂ pressure. However, it became increasingly evident at higher temperatures that the reaction order in CO₂ increased with increasing H₂ pressure on 5% Pd/Al₂O₃ (0.52–0.68 at 573 K) and, to a lesser extent, on 0.5% Pd/Al₂O₃ (0.49–0.57 at 593 K). In comparison, the reaction order in H₂ pressure increased less markedly with the increase in the partial pressure of CO₂ (10–50 kPa) for both catalysts. Noticeably, smaller reaction orders in H₂ were observed at higher temperatures, contrary to the trend observed for CO₂ reaction order. The effect of reaction temperature on the H₂ reaction order is most pronounced at the lowest CO₂ pressure studied (10 kPa). Variations in reaction orders are more pronounced on large Pd particles (5% Pd/Al₂O₃) than on small particles (0.5% Pd/Al₂O₃).

Table 2 shows the dependences of CH₄ formation rate on CO₂ and H₂ partial pressures for both catalysts. For CH₄ formation, the apparent reaction order in CO₂ was negative (~−0.2 – −0.1) regardless of Pd loading, gas compositions, and temperature. The CO₂ order became slightly less negative at higher temperatures, or with increasing H₂ pressure at a given temperature. The reaction order in H₂ varied from ~0.6 to ~0.7 on both catalysts, with higher values at higher CO₂ pressure or reaction temperature. The effect of temperature on the H₂ reaction order is more pronounced on small particles (0.5% Pd/Al₂O₃). The drastically different reaction orders in CO₂ and H₂ for CO and CH₄ formation (cf. Tables 1 and 2), along with the distinct barriers measured for both routes (Figure 2), clearly suggest that the two routes (CO₂ methanation and reverse water gas shift) do not share the same rate-determining step and reactive intermediates.

3.2. In Situ Transient DRIFTS-MS Measurements. In order to gain insight into the surface species present on the Pd/Al₂O₃ catalysts under different conditions, a series of DRIFTS measurements were carried out under transient conditions. We examined the formation of surface species from gas streams containing CO₂ and CO₂ + H₂ at 513 K, and subsequently, we monitored the conversion of the thus produced surface species by switching between different gas streams (He, H₂, or CO₂). The composition of the effluent gas was followed as a function of time by mass spectrometry (MS) during the entire experiment. Correlating the DRIFTS and MS results provides useful insight into the reaction sequence taking place under varying conditions, and helps to identify key surface species that are mechanistically relevant to the reduction of CO₂ by H₂ to different products on small and large Pd particles.

3.2.1. 5% Pd/Al₂O₃. A series of IR spectra recorded during CO₂ exposure and subsequent purge in He flow of a reduced 5% Pd/Al₂O₃ catalyst sample is displayed in Figure 3a. Prior to spectral acquisition at 513 K, the catalyst sample was reduced in H₂ at 673 K for 1 h and purged by He for 5 h at the same temperature to ensure the removal of all ad(ab)sorbed hydrogen from the Pd particles. The IR features developed during CO₂ exposure are related exclusively to adsorbed species on the alumina support, as well as to gas-phase CO₂ (2349 cm^{−1}), while no adsorbed CO species were seen on the Pd particles. The IR bands at 1230, 1442, and 1646 cm^{−1}^{20–23} represent different vibrational modes of adsorbed bicarbonates,

Table 1. Reaction Orders for CO Formation Rate in CO₂ and H₂ Pressures during CO₂ Hydrogenation on 5% and 0.5% Pd/Al₂O₃ at 513–593 K and Different Partial Pressures of CO₂ and H₂ (10–50 kPa for Both, Total Pressure 101 kPa Balanced with He)

catalyst	T/K	orders in CO ₂ with constant P _{H₂} / kPa					orders in H ₂ with constant P _{CO₂} / kPa				
		10	20	30	40	50	10	20	30	40	50
5% Pd/Al ₂ O ₃	513	0.48	0.47	0.45	0.46	0.48	0.21	0.21	0.22	0.22	0.21
	533	0.47	0.49	0.51	0.52	0.53	0.20	0.22	0.24	0.24	0.26
	553	0.49	0.52	0.55	0.57	0.60	0.13	0.18	0.20	0.22	0.22
	573	0.52	0.57	0.60	0.64	0.68	0.06	0.14	0.17	0.19	0.20
0.5% Pd/Al ₂ O ₃	533	0.42	0.45	0.44	0.44	0.46	0.21	0.22	0.22	0.23	0.24
	553	0.45	0.46	0.47	0.48	0.48	0.19	0.22	0.22	0.23	0.23
	573	0.47	0.49	0.50	0.51	0.52	0.19	0.20	0.22	0.22	0.23
	593	0.49	0.51	0.53	0.54	0.57	0.16	0.19	0.20	0.21	0.22

Table 2. Reaction Orders for CH₄ Formation Rate in CO₂ and H₂ Pressures during CO₂ Hydrogenation on 5% and 0.5% Pd/Al₂O₃ at 513–593 K and Different Partial Pressures of CO₂ and H₂ (10–50 kPa for Both, Total Pressure 101 kPa Balanced with He)

catalyst	T/K	orders in CO ₂ with constant P _{H₂} / kPa					orders in H ₂ with constant P _{CO₂} / kPa				
		10	20	30	40	50	10	20	30	40	50
5% Pd/Al ₂ O ₃	513	-0.21	-0.20	-0.19	-0.14	-0.15	0.60	0.61	0.61	0.65	0.67
	533	-0.20	-0.18	-0.17	-0.15	-0.13	0.66	0.65	0.65	0.67	0.72
	553	-0.19	-0.16	-0.17	-0.16	-0.12	0.61	0.63	0.65	0.67	0.68
	573	-0.17	-0.17	-0.15	-0.15	-0.11	0.63	0.67	0.69	0.70	0.72
0.5% Pd/Al ₂ O ₃	533	-0.22	-0.16	-0.14	-0.15	-0.15	0.55	0.57	0.55	0.57	0.59
	553	-0.17	-0.14	-0.11	-0.09	-0.07	0.59	0.63	0.66	0.68	0.70
	573	-0.14	-0.16	-0.13	-0.10	-0.10	0.67	0.71	0.75	0.75	0.78
	593	-0.20	-0.14	-0.11	-0.10	-0.10	0.62	0.66	0.68	0.72	0.74

and the 1525 cm⁻¹ peak is characteristic of carbonates.^{22–26} Detailed assignments of these species were discussed in our recent publications on Al₂O₃ and Pd/Al₂O₃ systems.^{27,28} Purging the IR cell with pure He resulted in a fast decrease and elimination of all the IR features representing adsorbed bicarbonates. A control experiment was performed where the reduced sample was cooled to 513 K in H₂ flow and briefly purged with He (instead of 673 K for 5 h); our aim was to prepare a catalyst that still contain ad(ab)sorbed hydrogen on(in) the metal particles. The series of IR spectra collected during the first 20 min of CO₂ exposure of this sample is presented in Figure 3b (black traces). Upon exposure of the hydrogen-containing catalyst to CO₂, an intense, broad band centered at 1909 cm⁻¹ with shoulders at both lower (1855 cm⁻¹) and higher (2050 cm⁻¹) wavenumber sides appeared, in addition to the IR features of the carbonates/bicarbonates on the alumina support. The 1909 cm⁻¹ peak, and the lower and higher frequency shoulders can be assigned to chemisorbed CO in bridging, 3-fold bound and linear forms, respectively.^{29,30} When CO₂ was removed from the gas feed by purging the cell with He (20–45 min; red traces, Figure 3b), the intensities of the IR features representing carbonates/bicarbonates decreased rapidly, while there were hardly any decreases in the intensities of the adsorbed CO bands. Introducing H₂ into the cell (t = 45 min) resulted in fast intensity decreases of all the IR features associated with adsorbed CO (blue traces in Figure 3b). Changes in the intensities of the IR bands of all the surface (adsorbed CO on Pd and carbonates/bicarbonates on the alumina support) and gaseous (CO_x) species, as well as the effluent gas composition, as monitored by MS, are presented as a function of time-on-stream in the top and bottom panels of Figure 3c, respectively. All IR absorption bands developed

rapidly and reached steady levels within a few minutes after the introduction of CO₂ into the IR cell. Note that the 28 amu MS signal in the first 20 min of time-on-stream in CO₂ completely accounts for the contribution of CO₂ from its fragmentation in the ionizer of the mass spectrometer, as no CO formation was detected by GC in the plug-flow reactor under the same conditions. No CH₄ formation was detected either in this time period. Following H₂ introduction (t = 45 min), a sharp decrease in the coverage of adsorbed CO was evidenced in the IR spectra, which coincided with the appearance of CH₄ (15 amu in MS) in the gas phase. The formation of CH₄ was also substantiated by its C–H stretching vibrational fingerprint at 3016 cm⁻¹ (Figure 3d). Furthermore, as soon as the IR signals of adsorbed CO disappeared, the formation of CH₄ ceased (Figure 3c).³¹

Next, the reduced 5% Pd/Al₂O₃ catalyst, kept at 513 K, was periodically exposed to H₂ and a gas stream containing CO₂ + H₂ (1:4 v/v), and the evolution of surface species and the gas-phase composition was followed as a function of time-on-stream by DRIFTS and MS, respectively (Figure 4). During the first 20 min of CO₂ + H₂ introduction onto the sample, compared with CO₂ exposure in Figure 3b, new intense IR features developed at 1376, 1393, and 1593 cm⁻¹, which are characteristic of adsorbed formate species on the surface of the alumina support (orange traces in Figure 4a).³⁰ The temporal evolution of different vibrational modes can be seen more clearly in Figure 4b (orange traces during the first 20 min in Figure 4a), which reveals the presence of alumina-bound bicarbonates (1230, 1438, and 1646 cm⁻¹) at the onset of CO₂ + H₂ exposure. However, these bands soon disappeared as the formate-related bands simultaneously grew more intense. Very strong IR bands of adsorbed CO (1845 and 1897 cm⁻¹)

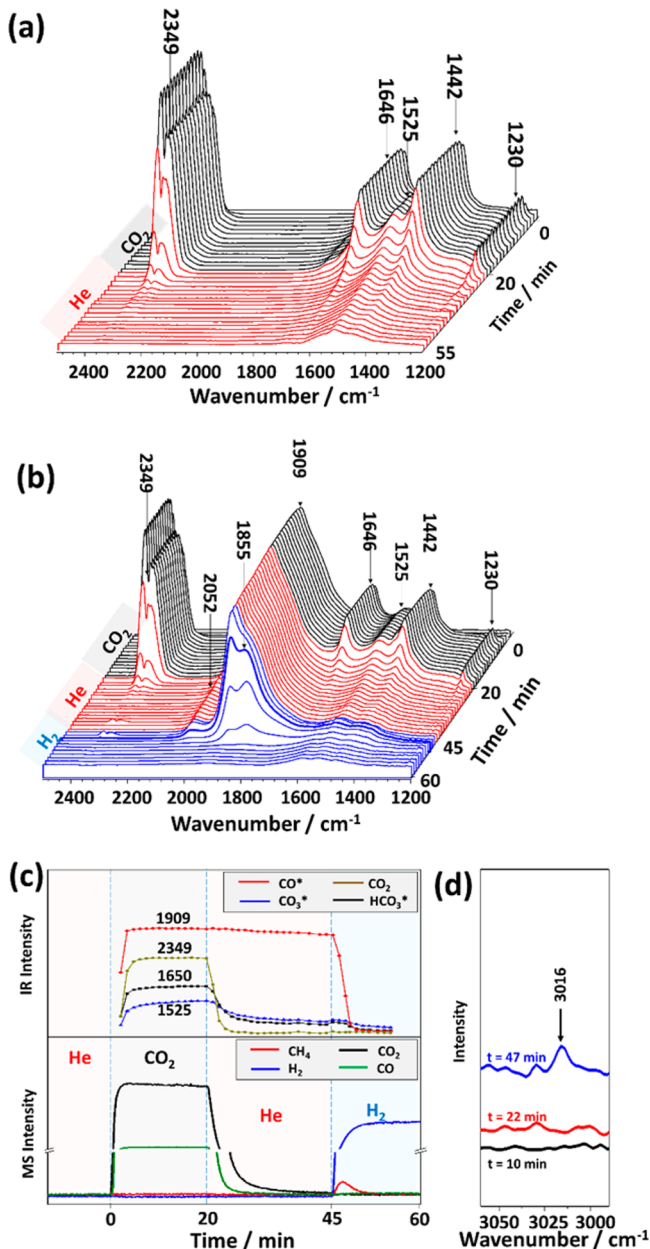


Figure 3. DRIFT spectra collected at 513 K when the feed gas was switched from He to CO₂, followed by a switch back to He over (a) reduced 5% Pd/Al₂O₃, and then to H₂ over (b,d) reduced 5% Pd/Al₂O₃ covered by pread(ab)sorbed H; (c) is the corresponding MS signals obtained at the exit of the DRIFT cell and IR band intensity of species in (b) as a function of time.

appeared in the IR spectrum even before the gas-phase CO₂ signal reached its plateau (2349 cm⁻¹), whereas the intensities of both surface bicarbonates and formates remained much weaker than bands associated with adsorbed CO over the entire 20 min. The bands centered at 1897 and 1845 cm⁻¹ are attributed to adsorbed CO in bridging and 3-fold configurations, respectively.^{29,30} With increasing CO coverage (longer CO₂+H₂ exposure time), this doublet feature, which developed into a broad band (1928 cm⁻¹ in Figure 4a) at longer CO₂+H₂ exposure times, also had a broad shoulder band at around 2050 cm⁻¹ representing linearly adsorbed CO. When the intensities of all IR bands reached stable levels (after 20 min exposure to CO₂+H₂ gas mixture), the feed gas was switched to H₂. The

spectra collected between 20 and 47 min (Figures 4a and 4c) clearly showed that the intensity of every IR feature decreased over time in H₂ flow. Gas phase CO₂ was completely purged out from the cell by the 27 min (also confirmed by the MS data displayed in Figure 4d). However, the intensity decrease of the IR bands representing adsorbed CO and formate with time-on-stream were much slower than that of gas-phase CO₂. The IR features of all three types of adsorbed CO completely disappeared by 40 min; in contrast, surface formates were much more stable than CO(ads) and were still present with appreciable intensities when the gas stream was switched back to CO₂+H₂ at 47 min. A closer inspection of the individual bands (Figure 4c) showed that the disappearance of linearly adsorbed CO (2050 cm⁻¹) was the fastest, followed by the bridging CO and the multiply bound ones at 1845 cm⁻¹. The different disappearance rates of adsorbed CO indicate that there are two types of bridging CO; one is at a high frequency 1945 cm⁻¹ (CO_{HF}) disappearing faster than the other one at low frequency 1920 cm⁻¹ (CO_{LF}). As the coverage of adsorbed CO decreased, the position of the 1920 cm⁻¹ IR feature (bridging CO) shifted to 1897 cm⁻¹, ultimately becoming a separate feature from the 1845 cm⁻¹ feature associated with CO bound to a 3-fold hollow site. Furthermore, the disappearance of the peak at 1656 cm⁻¹ due to monodentate formate species³² was as fast as that of adsorbed CO and much faster than that of the peak at 1593 cm⁻¹ attributed to bidentate formate. When the gas flow was switched back to CO₂+H₂ at 47 min, the intensities of all the adsorbed species recovered to the same level as they had been before switching from CO₂+H₂ to H₂.

Figure 4d shows the variations in the MS intensities of selected *m/z* channels over the entire course of the experiments in Figure 4a. Upon switching the gas feed from H₂ to CO₂+H₂ (*t* = 0), a surge in CH₄ formation rate was observed instantaneously, which dropped to a steady level after ~5 min time-on-stream. The freshly reduced Pd sample was populated with adsorbed (and absorbed) H, and when the gas was switched to CO₂+H₂, the initial rate for CH₄ formation in this transient or induction period should be higher than that at steady-state where the surface became partly covered by CO₂-derived intermediates. During the CO₂+H₂ reaction in 0–20 min, the formation of CO as a product could not be verified in MS, because CO₂ conversion was very low, and the signal of 28 amu from CO₂ fragmentation prevented us from distinguishing CO produced by the reaction. As the feed gas was switched back to H₂ at 20 min, the rate of CH₄ formation increased immediately and reached a maximum before gradually decreasing to a level below the detection limit of the MS. Because the reaction rate had a negative order in CO₂ (Table 2), the removal of CO₂ might have brought about this large increase (around the 20th min) in the CH₄ formation rate. However, one may notice that the decrease in CH₄ level in the effluent was much slower than the decrease in CO₂ level. At 27 min, there was no CO₂ signal present in either the IR or MS spectra. However, the production of CH₄ was still clearly visible long after the gas-phase CO₂ was completely removed from the IR cell (up to ~40 min). At about 40 min, the rate of CH₄ formation decreased to zero, coinciding with the disappearance of chemisorbed CO in the IR spectrum. As the gas stream was switched back to CO₂+H₂ again at 47 min, the MS signal of CH₄ directly reached its steady-state level without the sudden increase during the initial several minutes.

A series of IR spectra presented in Figure 5a shows the evolution of surface species on the 5% Pd/Al₂O₃ during

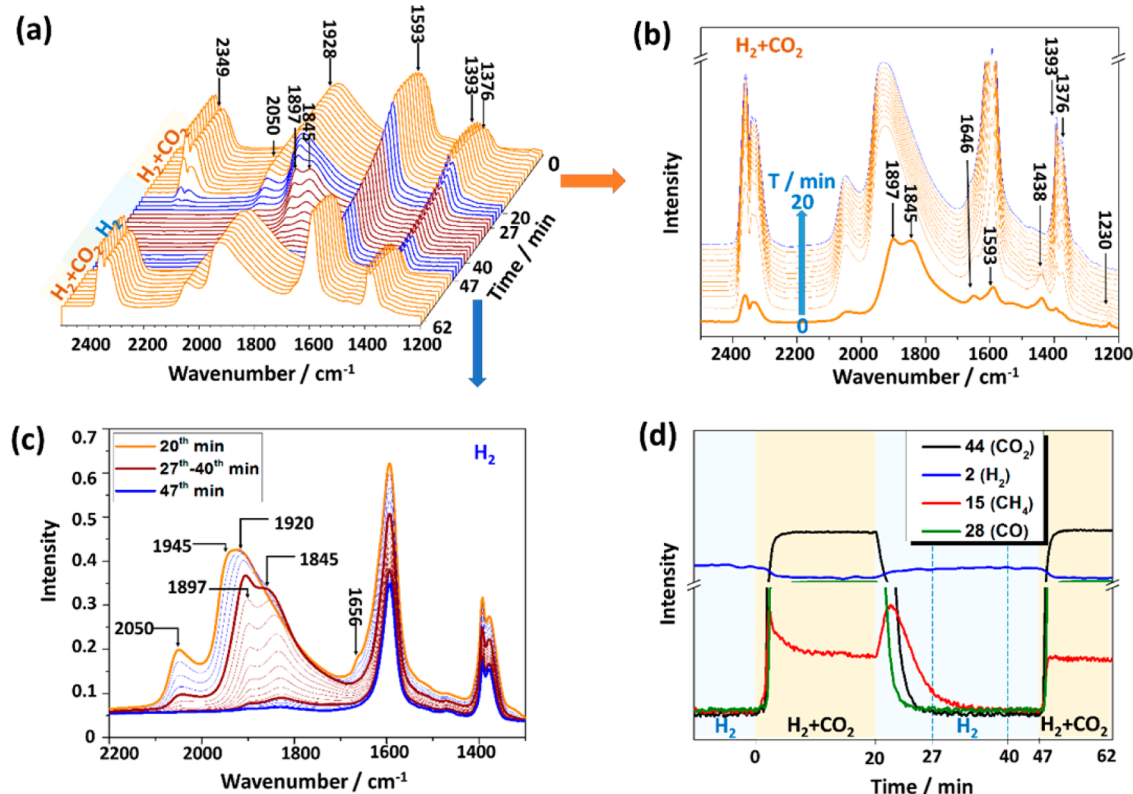


Figure 4. (a) DRIFT spectra and (d) the corresponding MS signals collected at the exit of the DRIFT cell as a function of time when the feed gas was switched from H₂ to CO₂ + H₂, followed by a switch back to H₂ then to CO₂ + H₂ again over 5% Pd/Al₂O₃ at 513 K. (b) DRIFT spectra during 0–20 min of (a) viewed in stacked traces. (c) DRIFT spectra during 20–47 min of (a) viewed in stacked traces.

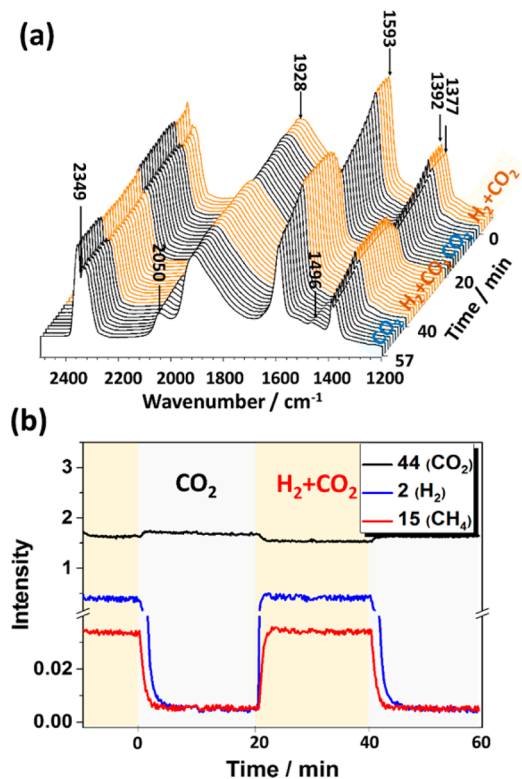


Figure 5. (a) DRIFT spectra and (b) the corresponding MS signals collected at the exit of the DRIFT cell as a function of time when the feed gas was switched alternately between CO₂ + H₂ and CO₂ over 5% Pd/Al₂O₃ at 513 K.

alternate switching between CO₂+H₂ (1:4 v/v) and CO₂-only feeds. The IR features present in the spectra collected under CO₂+H₂ flow were identical to those shown under the same conditions in Figure 4a: formate bands at 1377, 1392, and 1593 cm⁻¹, adsorbed CO showing broad bands at 1928 and 2050 cm⁻¹ and gaseous CO₂ at 2349 cm⁻¹. The intensities of IR bands representing adsorbed CO and gas-phase CO₂ did not change significantly after the switch from CO₂+H₂ to CO₂, while the signal of adsorbed formates gradually decreased. However, if one further takes a closer look at the spectra collected in the 0–20 min in CO₂ flow (shown in Figure S1a), the intensity of linear CO and bridging CO_{HF} band at 1942 cm⁻¹ slightly decreased and the 1656 cm⁻¹ band (monodentate formate) gradually disappeared while the intensity of the IR feature for bridging CO_{LF} stayed essentially constant. The intensities of formate and CO_{HF} bands recovered rapidly once the gas flow was switched back from CO₂ to CO₂+H₂. The online detection of the mass fragments (Figure 5b) clearly shows that the concentration of CH₄ produced in the CO₂+H₂ reaction decreased without any delay when the feed gas was switch to CO₂, and dropped to zero together with H₂ almost simultaneously. Moreover, when the gas flow was switched back CO₂+H₂ (t = 20 min), the CH₄ production was immediately re-established at the steady-state level.

In order to understand the interaction of CO with the 5% Pd/Al₂O₃ sample, the reduced sample was exposed to a flow of CO at 513 K. The series of IR spectra are displayed in Figure 6a as a function of CO exposure time. Adsorbed CO (1800–2060 cm⁻¹) was observed instantaneously, and the intensities of its IR signature features reached saturation (from the second spectrum) before any other adsorbed species were observed.

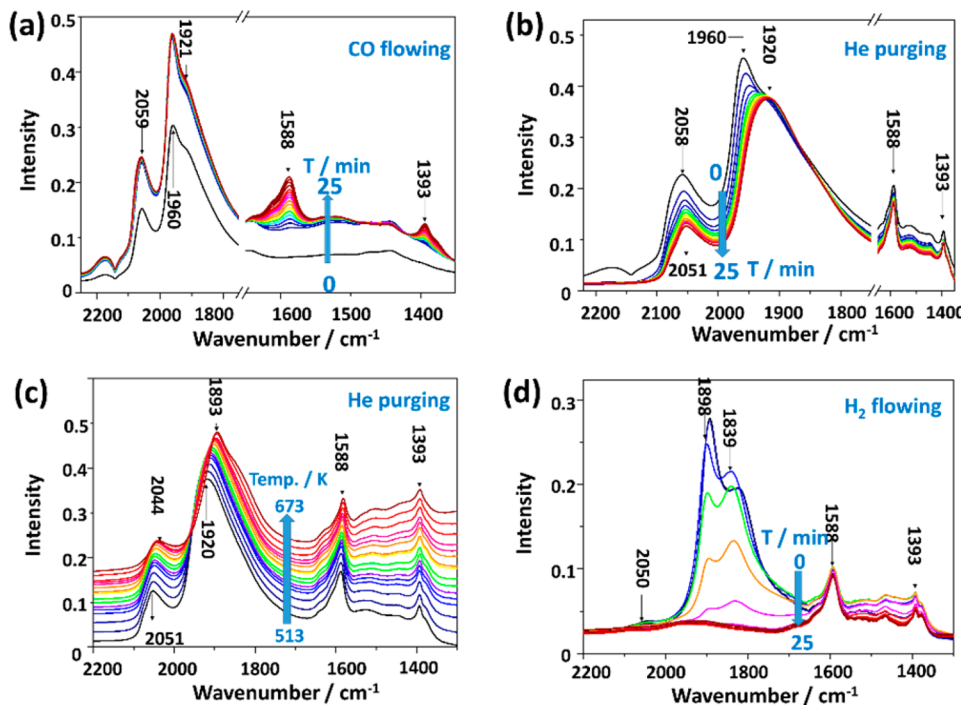


Figure 6. DRIFT spectra collected when the 5% Pd/Al₂O₃ (initially in H₂ flow) was exposed to (a) CO flow at 513 K, followed by a switch to (b) a He flow, then (c) with the temperature heated up to 673 K in the He flow, and finally (d) back to 513 K in the H₂ flow.

The peak at 2059 cm⁻¹ represents a linear adsorbed CO, while the 1960 cm⁻¹ peak and a 1921 cm⁻¹ shoulder are attributed to bridging-bound CO_{HF} and CO_{LF} species on metallic Pd, respectively. After saturation of the Pd surface with adsorbed CO, a slow formation of alumina-bound formate (1588 and 1393 cm⁻¹) was observed. After 25 min exposure to CO flow, the sample was purged with He, and the IR spectra collected during the He purge are shown in Figure 6b. With the disappearance of gas-phase CO from the system, the intensities of linearly (2058 cm⁻¹) and bridge-bound (1960 cm⁻¹) CO_{HF} decreased. As a result of the coverage decrease in linearly adsorbed CO, its frequency shifted from 2058 to 2051 cm⁻¹. On the other hand, the intensity of the IR feature of multiply bound CO (1920 cm⁻¹) did not decrease at all, exhibiting the same shape as seen for the adsorbed CO peak formed in CO₂+H₂ (Figures 4 and 5). Even after elevating the sample temperature to 673 K in He flow, all these IR peaks remained very stable (Figure 6c). In contrast, as soon as the gas flow was switched to H₂, at a decreased sample temperature of 513 K, the IR intensity of adsorbed CO rapidly decreased (Figure 6d). At the same time, the production of CH₄ was detected by MS (Figure S2). The intensities of the formate bands did not drop significantly during 25 min of H₂ exposure.

3.2.2. 0.5% Pd/Al₂O₃. In order to understand the effect of metal particle size on the nature and reactivity of surface species formed upon exposure to different gas environments, we conducted transient DRIFTS-MS measurements on a 0.5% Pd/Al₂O₃ sample under identical experimental conditions to those described above for the 5% Pd/Al₂O₃ catalyst.

The series of DRIFT spectra displayed in Figure 7 was collected under identical conditions to those described in Figure 3b. The H₂-reduced sample was briefly purged with He at 513 K and then exposed to a CO₂ flow (there was hydrogen ad(ab)sorbed on/in the Pd particles). Similarly to 5% Pd/Al₂O₃, IR features of bicarbonate/carbonate and adsorbed CO

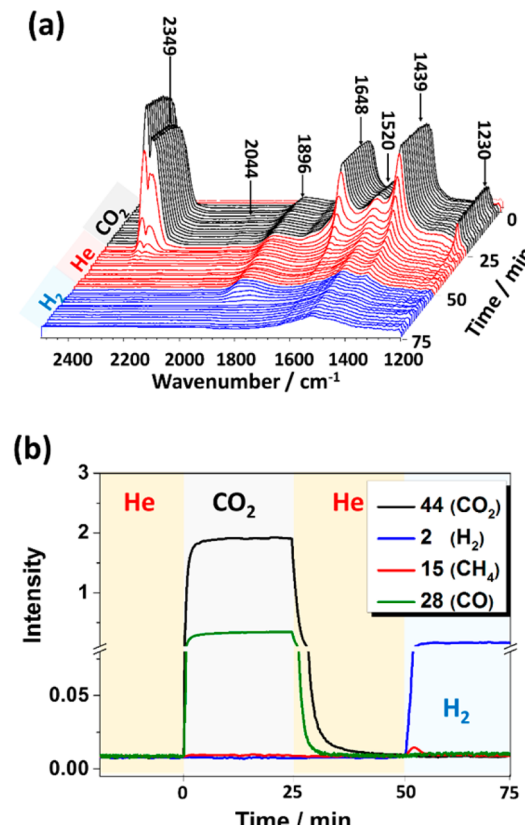


Figure 7. (a) DRIFT spectra and (b) the corresponding MS signals at the exit of the DRIFT cell collected at 513 K as a function of time when the feed gas He was switched from He to CO₂, followed by a switch back to He and then to H₂ over a reduced 0.5% Pd/Al₂O₃ sample covered with pread(ab)sorbed H.

developed rapidly on the surface of 0.5% Pd/Al₂O₃ upon its exposure to CO₂. The primary difference between the two sets of IR spectra (Figure 3b and Figure 7a) is that the intensities of bicarbonate (1650, 1439, and 1228 cm⁻¹) and carbonate (1525 cm⁻¹) bands are much higher than those of the adsorbed CO features (1896 and 2044 cm⁻¹) for the 0.5% Pd-containing sample. When the feed gas was switched from CO₂ to He, the IR intensities of the bicarbonate and carbonate features decreased rapidly, while no changes were observed in the intensities of adsorbed CO bands. After 25 min of He purge, the intensities of the peaks representing bicarbonate and carbonate species dropped to nearly zero. At this point, the feed gas was switched to H₂. The intensities of the bicarbonate and carbonate bands showed no more decrease, while the intensities of the bands of adsorbed CO decreased rapidly, and completely disappeared after ca. 10 min time-on-stream in H₂. The MS intensities of selected *m/z* channels during the course of this experiment are displayed in Figure 7b. After purging the CO₂-exposed sample with He for 20 min (*t* = 50 min) when H₂ was introduced into the DRIFTS cell, the formation of CH₄ was observed but no CO was detected. Concurrent with the disappearance of adsorbed CO signal in the IR spectra, the production of CH₄ ceased and the 15 amu MS signal dropped to the background level. Note that this phenomenon was exactly the same as that seen for 5% Pd/Al₂O₃, although the concentration of adsorbed CO on the surface of 0.5% Pd/Al₂O₃ was much smaller.

The series of IR spectra and the corresponding MS intensities of effluent gas on the 0.5% Pd/Al₂O₃ sample, as the feed gas was switched between H₂ and CO₂ + H₂ at 513 K, are displayed in Figure 8a and 8b, respectively. The exposure of the 0.5% Pd/Al₂O₃ sample to CO₂+H₂ resulted in the instantaneous development of IR features representing

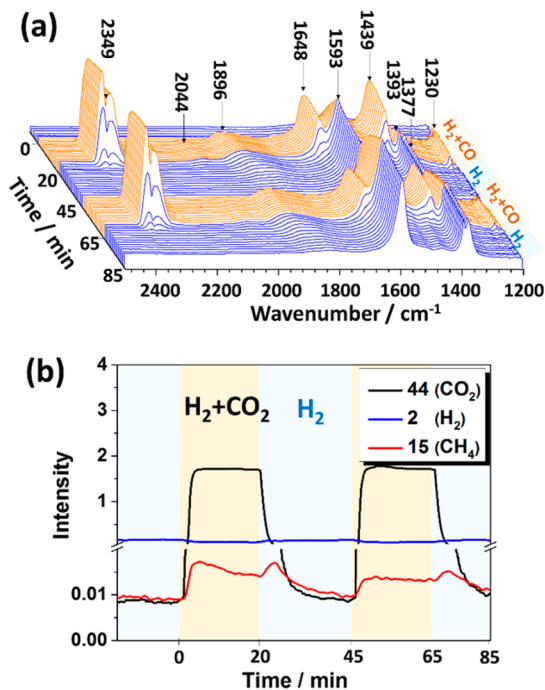


Figure 8. (a) DRIFT spectra and (b) the corresponding MS signals at the exit of the DRIFT cell collected at 513 K as a function of time when the feed gas was switched alternately between H₂ and CO₂+H₂ over a reduced 0.5% Pd/Al₂O₃ sample.

bicarbonates. After 2 min exposure, the integrated intensity of the ~1650 cm⁻¹ band reached its maximum and further exposure resulted in a slow, steady decline in the intensity of this IR feature (Figure S3). Concomitant with the decrease in the intensity of bicarbonate features was the development of IR bands of formate species. Furthermore, the signatures of adsorbed CO on Pd appeared at the same time as the bicarbonate bands (detailed in Figure S3). When the gas stream was switched from CO₂+H₂ to H₂ at 20 min, the intensities of all the bicarbonate features decreased rapidly, and disappeared after ca. 5 min in H₂ flow. At the same time, the intensity of the adsorbed CO band also decreased, though the decrease was much slower than that of the bicarbonate ones. As the intensity of the IR band of adsorbed CO decreased, its peak shifted to lower wavenumbers, as a result of a decrease in coverage. In the H₂ stream, the intensities of the formate species decreased rather slowly compared to those of adsorbed CO and bicarbonate. After 25 min in H₂ (*t* = 45 min), the gas flow was switched back to CO₂+H₂. The trends observed in the IR spectra after this switch were identical to those we have discussed above for the initial switch from H₂ to CO₂+H₂, that is, a rapid establishment of bicarbonate and adsorbed CO bands, and a slow evolution of formate features.

CH₄ formation was detected by MS immediately after the introduction of CO₂+H₂ into the IR cell (amu =15, Figure 8b). Similar to the observations on 5% Pd/Al₂O₃, the concentration of CH₄ in the effluent gas stream showed an initial overshoot, and then, after reaching a maximum, it decreased slowly to a stable level. When the feed gas was switched back to H₂ (*t* = 20 min), the concentration of CH₄ in the effluent increased immediately, reached a maximum, and then gradually decreased to the background level. The gas-phase concentration of CH₄ in the second CO₂ + H₂ cycle (45–65 min in Figure 8b) reached the steady-state level without the initial “overshooting”.

A series of IR spectra and the MS intensities of effluent gas on the 0.5% Pd/Al₂O₃ sample, as the feed gas was alternately switched between CO₂ + H₂ and CO₂ streams at 513 K, are shown in panels a and b, respectively, of Figure 9. The surface species detected were adsorbed CO on Pd, as well as bicarbonates and formates on the alumina support, under steady-state reaction conditions both in CO₂ + H₂ and CO₂ streams. In the presence of gas-phase CO₂ throughout this experiment, no large variations in the IR intensities of any of these adsorbed species (CO, bicarbonate, and carbonate) were observed, while the intensities of the formate bands continuously, but very slowly, increased over time (Figure S1b). The variation in MS signal intensities (Figure 9b) indicates that as H₂ was removed from the feed stream, the production of CH₄ ceased (*t* = 0 and 40 min), while the introduction of H₂ into CO₂ stream (*t* = 20 min) re-established the steady-state CH₄ production without any delay.

4. DISCUSSION

4.1. Kinetics of CO₂ Hydrogenation on Pd/Al₂O₃ Catalysts. First, we compare the turnover frequencies determined in this work with reported values in the literature on Pd particles under similar conditions. Solymosi and Erdőhelyi reported TOFs of 0.9×10^{-3} and 1.1×10^{-3} s⁻¹ for CO₂ hydrogenation to CH₄ and CO, respectively, on a Pd/Al₂O₃ catalyst ($D_{Pd} = 19.1\%$) at H₂/CO₂ = 4 and 548 K.³³ Although the selectivity to methane is lower than that to CO, consistent with our observations at temperatures below 600 K, both values (measured at 548 K) are substantially lower than

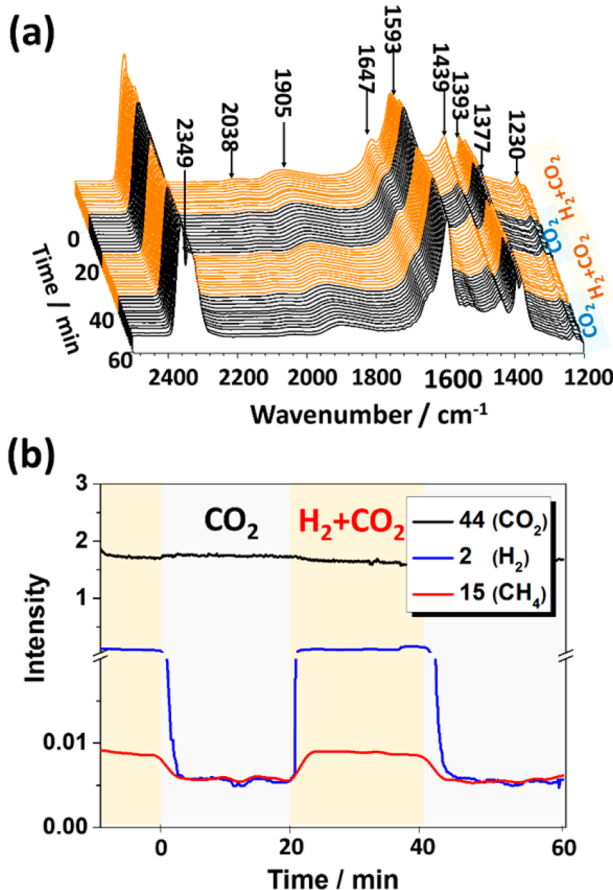


Figure 9. (a) DRIFT spectra and (b) the corresponding MS signals at the exit of the DRIFT cell collected at 513 K as a function of time when the feed gas was switched alternately between CO₂ + H₂ and CO₂ over a reduced 0.5% Pd/Al₂O₃ sample.

ours (TOFs at 553 K for methanation and CO formation: 8.6×10^{-3} and $2.1 \times 10^{-2} \text{ s}^{-1}$, respectively, on 5% Pd/Al₂O₃ with a dispersion of 11%). In a recent study, Al₂O₃ supported Pd catalyst with a dispersion of 16% showed CH₄ TOF is 2.42×10^{-3} at 573 K.³⁴ A series of supported Pd catalysts with different loadings, Pd dispersions and supports were also reported by Solymosi et al.³⁰ On Pd/Al₂O₃, the TOFs are $2.7 - 3.9 \times 10^{-3}$ for CH₄ formation and $0.25 - 37.4 \times 10^{-3} \text{ s}^{-1}$ for CO formation at 573 K, closer to those in the current study (TOFs at 573 K for CO formation: 1.2×10^{-2} and $2.7 \times 10^{-2} \text{ s}^{-1}$ on 0.5% and 5% Pd/Al₂O₃ catalysts, respectively; for methanation: 2.3×10^{-3} and $1.8 \times 10^{-2} \text{ s}^{-1}$ on the two catalysts). The selectivity to methane decreases with increasing Pd dispersion, qualitatively in agreement with this work (Section 3.1).

The apparent activation energy of CH₄ formation on Pd/Al₂O₃ has been reported to be in the range of 80–100 kJ/mol, and that of CO formation falls within 40–60 kJ/mol at a H₂/CO₂ reactant gas ratio of 4/1.^{30,34} At the same H₂/CO₂ ratio and in a similar temperature range, the measured energies of activation are 94 and 81 kJ/mol for CH₄ formation on 5% and 0.5% Pd/Al₂O₃, respectively, and 40 and 45 kJ/mol for CO formation on 5% and 0.5% Pd/Al₂O₃ (Figure 3), all values in good agreement with prior literature data.

Measured activation barriers for CO formation were similar for large and small metal particles at all conditions investigated, suggesting that the mechanism and energetics landscape for

CO formation from CO₂ does not vary with the dominant surface structure on Pd/Al₂O₃. In contrast, measured barriers for CH₄ formation were significantly lower on 0.5% Pd/Al₂O₃ with small Pd particles than on 5% Pd/Al₂O₃ with much larger Pd domains. This suggests that the reaction steps that primarily define the activation energies for CH₄ and CO formation occur on different parts of the catalyst, the metal and oxide support surfaces, respectively. On the contrary, apparent activation energy for CH₄ formation is observed to be lower on large Rh particles (61 kJ/mol, 15 nm) than on small ones (95 kJ/mol, 3.6 nm), which has been attributed by the authors to the prevalence of terraces that favor the rate-limiting step.⁷ Note that Solymosi and co-workers found no trends in the apparent energy of activation for CO₂ methanation with changing Pd particle size on a series of Pd/Al₂O₃ catalysts spanning a dispersion range of 4.4–40%. However, it is interesting that two of their catalysts with similar dispersions (19.6% and 18.7%) exhibited very different apparent activation energies (82 and 98 kJ/mol, respectively).³⁰

The power rate law for CO formation [$r_{\text{CO}} = k_1 P_{\text{CO}_2}^{(0.4-0.6)} P_{\text{H}_2}^{(0.1-0.3)}$] was virtually independent of Pd particle size (Tables 1 and 2), indicating the rate-determining step (RDS) for CO formation is possibly the same on both samples. Conceptually, the formation of bicarbonate/carbonate, which does not need the presence of H₂, cannot be the RDS, as it will be otherwise inconsistent with this rate expression which shows dependence on H₂ pressure. Both the transformation of bicarbonate/carbonate into formate and the decomposition of formate need to be assisted by hydrogen (later discussion based on IR spectroscopic evidence). However, merely based on the kinetic data, it remains uncertain which one is the RDS for CO formation on Pd/Al₂O₃. In the next section, we will discuss the spectroscopy observations presented earlier.

The power rate law for CH₄ formation [$r_{\text{CH}_4} = k_2 P_{\text{CO}_2}^{(-0.2 - 0.1)} P_{\text{H}_2}^{(0.6-0.8)}$], also independent of particle size, is characteristically distinct from that for CO formation in its negative CO₂ pressure dependence and much greater H₂ pressure dependence. Karelovic et al. also reported a negative order of −0.09 in CO₂ and a positive order of 0.81 in H₂, which is in good agreement with the results obtained in this study.³⁴ For the methanation reaction on Rh catalysts, the CO₂ partial pressure dependence was shown to vary, ranging from −0.46 to 0.4.^{8,35–37} The reaction order with respect to CO₂ pressure was negative for CH₄ formation, clearly indicating that one or some of the CO₂-derived intermediates inhibits the methanation pathway over our Pd-loaded catalysts. It is tempting to suggest that poisoning by CO might be the reason for this negative reaction order, and the possible role of CO as a poison in the methanation reaction¹³ will be discussed in the next section.

In summary, the different rate expressions and apparent energies of activation from our kinetic measurements have enabled us to conclude that CO and CH₄ formation do not share the same rate-limiting step. Taking together all the observations, we further propose that the reaction steps that primarily define the activation energies for CH₄ and CO formation occur on different parts of the catalyst, the metal and oxide support (or interfacial sites) surfaces, respectively, for which we provide spectroscopic evidence in the following paragraphs.

4.2. CO₂ Activation: Elementary Steps and Active Sites. The IR spectra shown in Figure 3a indicate that in the

absence of active hydrogen (associated with Pd) on the catalyst, CO_2 can only react with OH groups on the support to form bicarbonates, and this process is completely reversible at 513 K. Moreover, gas-phase CO was never detected by GC during CO_2 exposure of reduced, annealed catalysts. These results unambiguously demonstrate that direct dissociation of CO_2 to CO cannot occur on $\text{Pd}/\text{Al}_2\text{O}_3$ catalysts under the conditions applied in this study. In contrast to Pd-based catalysts, direct dissociation of CO_2 , leading to adsorbed CO, has been shown to be possible on other supported metal (Rh and Ru) catalysts.^{5,8,38} A critical point here is that the ad(ab)sorbed hydrogen must be completely removed from the reduced Pd catalyst (e.g., by extensive evacuation or purging at high temperatures such as 673 K) before CO_2 exposure. Residual hydrogen in the system (see IR spectra in Figure 3b and Figure 7a), in any form, may lead to the observation of adsorbed CO features in the IR spectra upon CO_2 exposure, indicating the need of H assistance for the dissociation of CO_2 or CO_2 -derived intermediates (e.g., bicarbonates).

All the DRIFTS results obtained in this work substantiate that the nature of the adsorbed species present on the two catalysts under $\text{CO}_2 + \text{H}_2$ stream is independent of the Pd particle size. These are adsorbed CO (linear, bridging, and multifold) on Pd, and bicarbonates/carbonates as well as formates on the Al_2O_3 support. A remarkable difference between these two catalysts is the rate of change in the surface concentration of bicarbonate species under reaction conditions. On 5% $\text{Pd}/\text{Al}_2\text{O}_3$, the formation of bicarbonates can only be seen in the first two IR spectra (Figure 4b). On the other hand, bicarbonate species were always present on 0.5% $\text{Pd}/\text{Al}_2\text{O}_3$ (Figure 8a). Moreover, these differences in the surface concentration of bicarbonates in $\text{CO}_2 + \text{H}_2$ at 513 K can be seen in Figure 10, where the normalized integrated intensities of the IR features representing bicarbonates, adsorbed CO and formates are plotted as a function of time-on-stream for both the 5% and 0.5% $\text{Pd}/\text{Al}_2\text{O}_3$ catalysts. The IR intensities of the bicarbonate bands increased rapidly and reached a maximum at the same time on both catalysts. However, on 5% $\text{Pd}/\text{Al}_2\text{O}_3$, the concentration of bicarbonates was far from its saturation level (the unity normalized integrated intensity in Figure 10a), while on 0.5% $\text{Pd}/\text{Al}_2\text{O}_3$, the bicarbonate was accumulated to nearly saturation concentration and then decreased slowly thereafter. Because the formation rate of bicarbonate depends on the CO_2 pressure, which should be identical for the two cases, the lower maximum bicarbonate concentration on 5% $\text{Pd}/\text{Al}_2\text{O}_3$ than that on 0.5% $\text{Pd}/\text{Al}_2\text{O}_3$ during CO_2 hydrogenation must be caused by the higher consumption rate of bicarbonate species on the former catalyst, which contains large Pd particles. The slower decomposition of bicarbonates on small Pd particles can only be explained either by a smaller kinetic rate constant (k) for the H-assisted bicarbonate decomposition or by a lower concentration of the involved H-species, or both. It seems more likely to us that there is a significant difference between the two catalysts in terms of the total concentration of available hydrogen species. The total concentration of the ad(b)sorbed H-species on 0.5% $\text{Pd}/\text{Al}_2\text{O}_3$ should be much lower than that on 5% $\text{Pd}/\text{Al}_2\text{O}_3$, at a level insufficient to fully consume the bicarbonates formed on the Al_2O_3 support.

In summary, our data show that the activation of CO_2 on both $\text{Pd}/\text{Al}_2\text{O}_3$ catalysts does not occur via direct dissociation to adsorbed CO and O; rather, it proceeds through a bicarbonate intermediate (on Al_2O_3), which, in turn, reacts

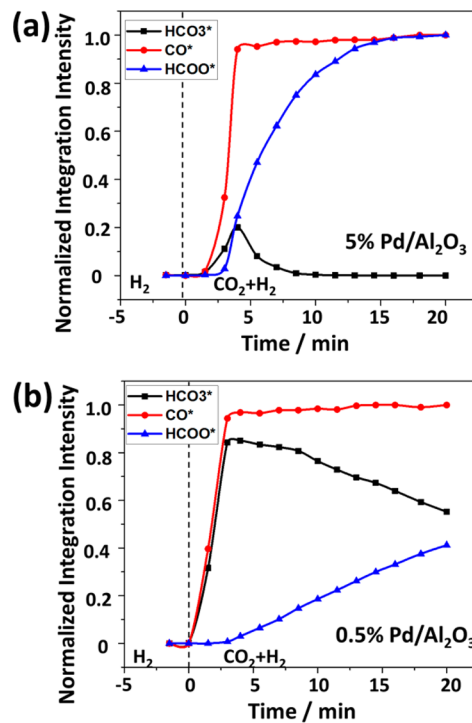


Figure 10. Normalized integrated intensity of adsorbed bicarbonate, CO and formate as functions of time when the feed gas was switched from H_2 to $\text{CO}_2 + \text{H}_2$ on (a) 5% $\text{Pd}/\text{Al}_2\text{O}_3$ and (b) 0.5% $\text{Pd}/\text{Al}_2\text{O}_3$ at 513 K. The integrated intensities of adsorbed bicarbonate, formate, and CO species at their respective saturation coverages were set as unity on each catalyst.

with ad(b)sorbed hydrogen species. In light of the evolution of different vibrational features related to bicarbonate and formate in the DRIFTS spectra (Figure S4), it seems likely that the intermediate directly formed from bicarbonates is a H-containing species (e.g., adsorbed formates).

4.3. Roles of Formates in CO_2 Hydrogenation. Next, we discuss the location and fate of formates. Formation of formates from H-assisted bicarbonate reduction has been clearly demonstrated in the previous section. Apparently, only Pd atoms can dissociate H_2 at this temperature; formate can then form at the interface between Pd and Al_2O_3 where H atoms are directly provided from nearby Pd sites to the bicarbonates. Alternatively, it is conceptually also viable that dissociated H atoms can spillover to, and react on, the support sites where bicarbonate is bound, leading to formate formation on the support. Interfacial sites between Pd and Al_2O_3 have been suggested for the reaction of formate which mainly anchors on the support, as was proposed also on other catalysts.^{1,11,39,40}

IR spectra shown in Figure 4 clearly reveal that formates can be slowly decomposed in H_2 . In a control experiment, gas-phase CO was detected when a sample prepopulated with formate was exposed to a stream of H_2 . In contrast, when this formate-covered sample was exposed to pure He, no CO formation was observed by either GC or MS. At substantially higher temperatures, surface formates may decompose as well at an appreciable rate in the absence of H_2 , but at this temperature (513 K), the reaction of formates with hydrogen is the only detectable route that produces CO.

In order to compare the reactivity of formates on 5% and 0.5% $\text{Pd}/\text{Al}_2\text{O}_3$, we plotted the intensities of the formate species (produced in $\text{CO}_2 + \text{H}_2$ gas mixture) as a function of

time of H₂ exposure on the two catalysts in Figure S5. The consumption rate of formates on 5% Pd/Al₂O₃ was much higher than that on 0.5% Pd/Al₂O₃. The reasons might be the same as for bicarbonate decomposition as discussed previously; the higher Pd loading on 5% Pd/Al₂O₃ can provide a larger total concentration of activated hydrogen species than that on the 0.5% Pd/Al₂O₃ catalyst for facilitating formate decomposition (reduction to CO).

The presence of monodentate formate (IR feature at ~1656 cm⁻¹) was observed on the 5% Pd/Al₂O₃ catalysts but not on the 0.5% Pd/Al₂O₃ sample in CO₂ + H₂ flow (Figure S1). These monodentate formates are less stable than bidentate formates; therefore, they disappeared rapidly when the feed gas was switched from CO₂ + H₂ to H₂. These observations suggest that these monodentate formates, located around the Pd particles, are more active than bidentate formates. Similar adsorbed species (monodentate formates) were reported recently to be the key intermediates in the decomposition of CH₃OH on Pd₂Ga/Ga₂O₃ catalysts.³²

CO is the sole product that forms in the reaction between formates on the Al₂O₃ and H atoms on the Pd particles. Our kinetic analysis shows that high partial pressure of H₂ will decrease the activation barrier for CO formation on both 0.5% and 5% Pd/Al₂O₃ catalysts. This agrees well with the fact that a higher concentration of ad(ab)sorbed H enhances the dissociation of formates. It is also expected that higher H₂ partial pressures lead to higher concentrations of dissociatively adsorbed hydrogen, which may, consequently, decrease the coverage of adsorbed CO species. If the desorption of CO was the rate-determining step for CO formation, a high H₂ pressure should lead to an increase in CO activation energy, in conflict with our observation. Accordingly, it is proposed that the activation barrier for CO formation originates mainly from the energy required to dissociate formates. Furthermore, the similarities in both activation energies and reaction orders for the formation of CO with varying partial pressures of CO₂ and H₂ on both 0.5% and 5% Pd/Al₂O₃ indicate that the different consumption rates of formates in H₂ flow are most likely due to the different concentrations of available hydrogen species, rather than the different rate constants for the decomposition of formates.

4.4. Chemisorbed CO as an Intermediate to CH₄.

Chemisorbed CO, the product of formate reduction, was mainly in multiply bound forms (bridging and 3-fold hollow) on the Pd particles at 513 K, exhibiting IR vibrational features in the 2000–1700 cm⁻¹ range on both 5% and 0.5% Pd/Al₂O₃ catalysts. The bridging CO_{LF} appearing as a shoulder at 1920 cm⁻¹, lower than the typical bridging CO_{HF} frequency (e.g., 1945–1960 cm⁻¹), is also observed by others. For example, Erdőhelyi et al. found that in the presence of H₂, the peak position of the IR band of adsorbed CO shift toward lower frequencies, caused by the electron transfer from the adsorbed H to the CO through Pd.³⁰ This charge transfer is claimed to increase the Pd–C bond strength and, concomitantly, to weaken the C–O bond, and they proposed the formation of Pd-carbonyl hydride species. This shift to lower frequencies due to coadsorbed H was also observed on other supported metal catalysts.⁴⁰ This type of CO(ads) is most probably responsible for the CO_{LF} discussed above.

CO adsorbed in linear at ca. 2050 cm⁻¹ and bridged configuration at 1945–1960 cm⁻¹ (CO_{HF}) showed lower stabilities (see, e.g., Figure 6) than those represented by the CO_{LF} (~1850–1920 cm⁻¹), presumably bound to 3-fold

hollow sites and/or bridging CO on Pd-hydrides. Those CO_{HF} with IR absorption at 1945–1960 cm⁻¹ were not stable; under He purge at reaction conditions, they desorbed and equilibrated with gaseous CO (Figures 6a,b and S1). In contrast, the results in Figures 3b, 6b, 6c, 7a and S1 provided strong evidence that the CO_{LF}, that is, the band centered at 1920 cm⁻¹, which stayed constant during He purge, was hard to desorb from the surface and did not equilibrate with gaseous CO; instead, such adsorbed CO_{LF} species with a longer surface lifetime would react further with dissociated hydrogen. Therefore, the observed CO features in IR are mainly due to the CO_{LF} more strongly held to the surface of Pd particles. Furthermore, CH₄ was detected as the only product by MS with the CO_{LF} as the sole surface species in H₂ (Figure 3b and 7a), indicating that these adsorbed CO_{LF} species (having a significantly weakened C–O bond) is the intermediate to CH₄ production.

The intensities of IR bands of adsorbed CO (mainly in multibound forms) on the 5% Pd/Al₂O₃ catalysts are much higher than that on the 0.5% Pd/Al₂O₃, due to the higher number of large metal particles present on the highly Pd-loaded sample. The larger metal particles provide a larger fraction of extended surfaces where it is easier to form multibound CO than on smaller particles. Because the CO_{LF} species is the key intermediate to CH₄ production, the direct reason for the vastly different selectivities to CO and CH₄ on the two Pd/Al₂O₃ catalysts¹⁷ most probably originates from the lower concentration of CO_{LF} species on 0.5% Pd/Al₂O₃.

Weatherbee et al. found that the product CO from CO₂ reduction acts as a poison for CH₄ production on Ni/SiO₂ catalyst.¹³ When CO is introduced into the feed stream, the formation of CH₄ is suppressed. On the contrary, we showed that low-frequency adsorbed CO were, in fact, important intermediates to CH₄. Our kinetic analysis (discussed in Section 4.1) also hints that the active sites for CO and CH₄ production are different. What really happens in this system is the competition for adsorption sites on the metal particles between CO_{HF} and hydrogen. With increasing CO partial pressure, most of the metal particles are covered by adsorbed CO (as evidenced from the increasing concentration of high-frequency adsorbed CO_{HF}; Figure 6) suppressing the dissociation of H₂ and consequently decreasing the surface coverage of atomic H. However, the dissociation of CO and the formation of CH₄ require sufficient coverage of atomic hydrogen on the metal surface, and once the H(ads) coverage drops to a certain level (due to the high CO(ads) coverage), the CH₄ formation rate will start to decrease. This, in turn, suggests that a delicate balance between the surface coverages of CO and H is required on the Pd particles to maximize CH₄ production. The insights gathered above, which point to the importance of terrace sites, allow us to predict that supported catalysts with large metal particles and/or high metal loadings, which are capable of activating CO₂ (forming bicarbonates on the support), are favorable choices for catalyzing CO₂ methanation at a high rate.

4.5. Plausible Mechanism of CO₂ Hydrogenation over Pd/Al₂O₃.

Both the steady-state kinetic data (activation energies, reaction orders in CO₂ and H₂ partial pressures) and the IR spectra under transient and steady-state conditions suggest no considerable difference in the prevailing mechanisms for CO₂ hydrogenation to CO and CH₄ on 5% and 0.5% Pd/Al₂O₃ catalysts, containing large and small metal particles, respectively. The catalytic reaction proceeds via a truly

bifunctional pathway, meaning that both the catalyst support (alumina) and the active metal particles (Pd) play critical roles in the activation of CO₂ and H₂. CO₂ cannot dissociate directly over the metallic Pd at these temperatures (<600 K), but it has to first react with the hydroxyls on Al₂O₃ to form bicarbonates. This reaction is very facile on alumina,^{27,28} and requires no metal particle participation. All the subsequent reaction steps, however, can proceed only in the presence of sufficient amount of adsorbed (atomic) hydrogen on the metal particles. The first step of the overall CO₂ reduction process is the cleavage of one C–O bond in bicarbonates to form formates. In the subsequent steps, formates are reduced by hydrogen to produce adsorbed CO species which tend to first populate highly coordinated Pd sites, showing a low frequency (CO_{LF}) IR band. Once these sites are saturated, linearly adsorbed CO (2050 cm⁻¹) and other less strongly held forms of adsorbed CO_{HF} (1960–1945 cm⁻¹) are formed and can easily desorb to gas-phase CO (Figure 6). As noted earlier, it seems more likely that formate decomposition, rather than bicarbonate decomposition, limits the rate of CO formation, on both small and large Pd particles. At the typical reaction temperature, only those adsorbed CO (in linear, bridging and 3-fold bound forms and likely associated with coadsorbed H (e.g., a Pd-carbonyl hydride species)), which show lower C–O stretching vibrational frequencies, are sufficiently stable on the surface and have sufficiently weakened C–O bond to allow further hydrogenation to methane. The fate of such CO_{LF} species depends on the availability of Pd-associated hydrogen species on(in) the catalyst.

Regarding further hydrogenation of CO_{LF} to methane, two main paths have been shown to exist: (i) direct dissociation of CO and (ii) H-assisted dissociation of CO, both having been widely debated in previous studies. Direct CO dissociation has been proposed to occur over group VIII metal-based catalyst.^{13,36} Recent density functional theory calculations, however, showed that the dissociation barrier of C–O bond is lower in COH (or CHO) intermediate than in CO(ads).⁴¹ Our results seem to suggest that further hydrogenation of CO_{LF} proceeds through an intermediate containing C, O, and H (e.g., formyl) rather than a direct dissociation pathway on Pd/Al₂O₃. The rate-limiting step for CH₄ formation is proposed to be the C–O bond breaking in the CO_{LF} species with hydrogen assistance. While desorption of CO and CH₄ regenerates the surface Pd sites, there must also be steps that regenerate support hydroxyls, consumed initially in the CO₂ activation step (i.e., bicarbonate formation), to fully close the catalytic cycle. Conceptually feasible pathways are the H-assisted dissociation of bicarbonate and/or formate and/or CO to produce OH_{ads}. The thus formed OH_{ads} can either activate another CO₂ or react with an adsorbed H to form water.

On the basis of the above understanding, we are able to redefine the TOFs for CO and CH₄ formation on the two Pd catalysts as the rates normalized to the concentration of a known type of surface sites which lead to the production of a specific product. For example, at 513 K, the concentration of surface sites that bind CO_{LF} species, leading eventually to CH₄ formation, was estimated (from the deconvolution and integration) to be an order of magnitude higher on 5% Pd/Al₂O₃ than that on 0.5% Pd/Al₂O₃. Although the TOFs, typically calculated on the basis of the number of surface atoms, were ~7–8 times higher on the 5% Pd/Al₂O₃ catalyst than on 0.5% Pd/Al₂O₃ (Figure 1), the two catalysts would actually have a comparable redefined TOF, normalized to the

concentration of CO_{LF}. Further studies are currently underway toward understanding, in greater depth, the nature, concentrations, and lifetimes of key surface species that mediate CO and methane formation, as well as probing the kinetic relevance and reversibility of different elementary steps on small and large Pd particles.

5. CONCLUSION

Under the studied reaction conditions, the mechanistic sequence for and the surface species involved in CO₂ hydrogenation do not change with the size of Pd particles. CO₂ does not dissociate directly to CO* and O* on Pd/Al₂O₃ catalysts; instead, it first reacts with a hydroxyl on Al₂O₃ to form a bicarbonate, which, in turn, reacts with ad(ab)sorbed hydrogen species to yield a formate. The decomposition of formate to CO ad-species also needs the assistance of ad(ab)sorbed hydrogen. The pathways for CO and CH₄ formation do not share the same rate-determining step and are favored by different surface structures. The Pd sites that hardly retain CO surface species formed from formate are more prevalent on the surface of smaller Pd particles, which exhibit a higher selectivity to gaseous CO product. In contrast, larger Pd particles, due to a higher population of those terrace sites where it is easier to form multibound CO and dissociated H is bound in the vicinity of CO, show a stronger interaction with CO. These stable CO species are mainly in multibound forms and are the direct intermediates to CH₄. The higher concentration of these reactive intermediates on large Pd particles results in an enhanced rate and selectivity along the methanation pathway.

Given the stronger CO adsorption than H adsorption on Pd particles and the necessity of H-assistance in the dissociation of C–O bonds in bicarbonate, formate and adsorbed CO species, an abundant supply of H species is a key requirement for maximizing CH₄ production during CO₂ hydrogenation on supported Pd catalysts. Aiming at higher CO₂ methanation rates, we envision that a rational step forward should be the tailored design and the synthesis of Pd catalysts with higher concentrations of terrace sites, which better activate the C–O bond, and/or high metal loadings, which increase the concentration of H-species.

■ ASSOCIATED CONTENT

S Supporting Information

The Supporting Information is available free of charge on the ACS Publications website at DOI: 10.1021/acscatal.5b01464.

DRIFT spectra, MS signal collected when different feed gases were switched over 5% and 0.5% Pd/Al₂O₃ (PDF)

■ AUTHOR INFORMATION

Corresponding Author

*E-mail: janos.szanyi@pnnl.gov.

Notes

The authors declare no competing financial interest.

■ ACKNOWLEDGMENTS

The catalyst preparation and catalytic measurements were supported by a Laboratory Directed Research and Development (LDRD) project. J.S. gratefully acknowledges the financial support of this work by the U.S. Department of Energy (DOE), Office of Science, Office of Basic Energy Sciences, Chemical Sciences, Geosciences, and Biosciences Division. J.H.K. also

acknowledges the support of this work by the 2015 Research Fund of UNIST (Ulsan National Institute of Science and Technology, Ulsan, Korea). The authors thank Dr. Davide Ferri (Paul Scherrer Institute, Switzerland) for the fruitful discussions on the reaction mechanism of CO₂ hydrogenation.

■ REFERENCES

- (1) Wang, W.; Wang, S. P.; Ma, X. B.; Gong, J. L. *Chem. Soc. Rev.* **2011**, *40*, 3703–3727.
- (2) Prairie, M. R.; Renken, A.; Highfield, J. G.; Thampi, K. R.; Gratzel, M. *J. Catal.* **1991**, *129*, 130–144.
- (3) Kim, H. Y.; Lee, H. M.; Park, J. N. *J. Phys. Chem. C* **2010**, *114*, 7128–7131.
- (4) Park, J. N.; McFarland, E. W. *J. Catal.* **2009**, *266*, 92–97.
- (5) Liotta, L. F.; Martin, G. A.; Deganello, G. *J. Catal.* **1996**, *164*, 322–333.
- (6) Vesselli, E.; Rizzi, M.; De Rogatis, L.; Ding, X. L.; Baraldi, A.; Comelli, G.; Savio, L.; Vattuone, L.; Rocca, M.; Fornasiero, P.; Baldereschi, A.; Peressi, M. *J. Phys. Chem. Lett.* **2010**, *1*, 402–406.
- (7) Karelovic, A.; Ruiz, P. *Appl. Catal., B* **2012**, *113*, 237–249.
- (8) Fisher, I. A.; Bell, A. T. *J. Catal.* **1996**, *162*, 54–65.
- (9) Falconer, J. L.; Zagli, A. *E. J. Catal.* **1980**, *62*, 280–285.
- (10) Lapidus, A. L.; Gaidai, N. A.; Nekrasov, N. V.; Tishkova, L. A.; Agafonov, Y. A.; Myshenkova, T. N. *Pet. Chem.* **2007**, *47*, 75–82.
- (11) Marwood, M.; Doepper, R.; Renken, A. *Appl. Catal., A* **1997**, *151*, 223–246.
- (12) Peebles, D. E.; Goodman, D. W.; White, J. M. *J. Phys. Chem.* **1983**, *87*, 4378–4387.
- (13) Weatherbee, G. D.; Bartholomew, C. H. *J. Catal.* **1982**, *77*, 460–472.
- (14) Fujita, S.; Terunuma, H.; Kobayashi, H.; Takezawa, N. *React. Kinet. Catal. Lett.* **1987**, *33*, 179–184.
- (15) Schild, C.; Wokaun, A.; Baiker, A. *J. Mol. Catal.* **1990**, *63*, 243–254.
- (16) Aldana, P. A. U.; Ocampo, F.; Kobl, K.; Louis, B.; Thibault-Starzyk, F.; Daturi, M.; Bazin, P.; Thomas, S.; Roger, A. C. *Catal. Today* **2013**, *215*, 201–207.
- (17) Kwak, J. H.; Kovarik, L.; Szanyi, J. *ACS Catal.* **2013**, *3*, 2094–2100.
- (18) Kwak, J. H.; Kovarik, L.; Szanyi, J. *ACS Catal.* **2013**, *3*, 2449–2455.
- (19) Koros, R. M.; Nowak, E. J. *Chem. Eng. Sci.* **1967**, *22*, 470.
- (20) Morterra, C.; Zecchina, A.; Coluccia, S.; Chiorino, A. *J. Chem. Soc., Faraday Trans. 1* **1977**, *73*, 1544–1560.
- (21) Vimont, A.; Lavalle, J. C.; Sahibed-Dine, A.; Arean, C. O.; Delgado, M. R.; Daturi, M. *J. Phys. Chem. B* **2005**, *109*, 9656–9664.
- (22) Morterra, C.; Magnacca, G. *Catal. Today* **1996**, *27*, 497–532.
- (23) Turek, A. M.; Wachs, I. E.; Decanio, E. *J. Phys. Chem.* **1992**, *96*, 5000–5007.
- (24) Peri, J. B. *J. Phys. Chem.* **1966**, *70*, 3168–3179.
- (25) Morterra, C.; Orio, L. *Mater. Chem. Phys.* **1990**, *24*, 247–268.
- (26) Parkyns, N. D. *J. Phys. Chem.* **1971**, *75*, 526–531.
- (27) Szanyi, J.; Kwak, J. H. *Phys. Chem. Chem. Phys.* **2014**, *16*, 15117–15125.
- (28) Szanyi, J.; Kwak, J. H. *Phys. Chem. Chem. Phys.* **2014**, *16*, 15126–15138.
- (29) Schild, C.; Wokaun, A.; Baiker, A. *J. Mol. Catal.* **1991**, *69*, 347–357.
- (30) Erdohelyi, A.; Pasztor, M.; Solymosi, F. *J. Catal.* **1986**, *98*, 166–177.
- (31) Weng, W. Z.; Chen, M. S.; Yan, Q. G.; Wu, T. H.; Chao, Z. S.; Liao, Y. Y.; Wan, H. L. *Catal. Today* **2000**, *63*, 317–326.
- (32) Hagofer, A.; Ferri, D.; Fottinger, K.; Rupprechter, G. *ACS Catal.* **2012**, *2*, 2305–2315.
- (33) Solymosi, F.; Erdohelyi, A. *J. Mol. Catal.* **1980**, *8*, 471–474.
- (34) Karelovic, A.; Ruiz, P. *ACS Catal.* **2013**, *3*, 2799–2812.
- (35) Iizuka, T.; Tanaka, Y.; Tanabe, K. *J. Catal.* **1982**, *76*, 1–8.
- (36) Solymosi, F.; Erdohelyi, A.; Bansagi, T. *J. Catal.* **1981**, *68*, 371–382.
- (37) Karelovic, A.; Ruiz, P. *J. Catal.* **2013**, *301*, 141–153.
- (38) Eckle, S.; Denkwitz, Y.; Behm, R. J. *J. Catal.* **2010**, *269*, 255–268.
- (39) Panagiotopoulou, P.; Kondarides, D. I.; Verykios, X. E. *J. Phys. Chem. C* **2011**, *115*, 1220–1230.
- (40) Solymosi, F.; Erdohelyi, A.; Bansagi, T. *J. Chem. Soc., Faraday Trans. 1* **1981**, *77*, 2645–2657.
- (41) Zhang, S. T.; Yan, H.; Wei, M.; Evans, D. G.; Duan, X. *RSC Adv.* **2014**, *4*, 30241–30249.